Neuron, Vol. 14, 1273–1283, June, 1995, Copyright © 1995 by Cell Press

Tonic Inhibition Originates from Synapses Close to the Soma

I. Soltesz,*† D. K. Smetters,‡ and I. Mody*§
*Department of Anesthesiology and Pain Management
University of Texas Southwestern Medical Center
Dallas, Texas 75235
†Department of Anatomy and Neurobiology
University of California at Irvine
Irvine, California 92717
‡Department of Brain and Cognitive Sciences
Massachusetts Institute of Technology
Cambridge, Massachusetts 02139

Summary

Central neurons are subject to a tonic barrage of randomly occurring spontaneous inhibitory events (mIPSCs) resulting from the action potential–independent release of γ-aminobutyric acid (GABA). Do the terminals making synapses onto somatic versus dendritic sites, which arise from specific populations of interneurons, differ in their ability to generate mIPSCs? We have combined the techniques of whole-cell patch-clamp recording and computational simulation to demonstrate that in granule cells of the dentate gyrus, most of the action potential–independent inhibition taking place as mIPSCs originates from proximal sites. Indeed, removal of the bulk (>50%) of the dendritic tree did not change the characteristics of mIPSCs. These results are consistent with a functional segregation of GABAergic terminals synapsing at proximal versus distal portions of central neurons. Thus, proximal GABAergic terminals are responsible for tonic inhibition targeted at the soma.

Introduction

On most principal cells of the cortex, inhibitory terminals originating from distinct interneuron types specifically innervate spatially segregated parts of the neuron, such as the axon initial segment, soma, and various parts of the dendrites. In the case of granule cells of the hippocampal dentate gyrus, this inhibitory innervation arises from at least five types of GABAergic neuron (Halasy and Somogyi, 1993b; Han et al., 1993). These interneurons terminate on, for the most part, mutually exclusive domains along the longitudinal axis of granule cells. The high specificity of their target selection makes it possible to predict the origin of GABAergic terminals from their location on the surface of granule cells (Han et al., 1993; Nusser et al., 1995). For example, axo-axonic or chandelier cells exclusively innervate the axon initial segment, whereas basket cells make contact with the somata and proximal dendrites of granule cells. These interneurons evoke short-latency, fast, $GABA_A$ receptor–mediated inhibitory synaptic events (Buhl et al., 1994a, 1994b). The inhibitory innervation of the dendrites is supplied by other cells classified according to the characteristic high specificity of their axonal and dendritic domains (Han et al., 1993). These include a type of hilar cell forming a dense axonal plexus in the inner third of the molecular layer (the termination zone of commissural and associational pathways), other hilar cells with axons in the outer two-thirds of the molecular layer (the termination zone of the perforant pathway from the entorhinal cortex), as well as a molecular layer cell type that terminates exclusively in the distal dendritic region of granule cells. The dendritic trees of these interneuron types can also occupy nonoverlapping domains. For example, the hilar neuron with axons in the outer two-thirds of the molecular layer has its dendrites restricted to the hilus, indicating that it is devoid of direct cortical inputs, whereas basket and axo-axonic cells have dendrites in the termination zone of perforant path fibers. Such a strict spatial segregation of the inputs and outputs of these GABAergic neurons raises the possibility that distinct inhibitory inputs to granule cells may play different functional roles (Nicoll, 1994).

Ultrastructural studies in the dentate gyrus have provided evidence for dendritic inhibition being as abundant, or even more abundant, than somatic inhibition. The numerical density of GABAergic synapses is similar in the somatic and dendritic regions of granule cells (Halasy and Somogyi, 1993a), which, combined with the greater volume of the dendritic layer, implies that granule cells probably receive the majority of inhibitory synapses on their dendrites. Immunocytochemical studies have demonstrated the presence of several of the α as well as β2/3, γ2, and δ type $GABA_A$ receptor subunits in both dendritic and somatic layers (Schoch et al., 1985; Richards et al., 1987; Houser et al., 1988; Benke et al., 1991; Zimprich et al., 1991; Turner et al., 1993; Gao and Fritschy, 1994; Gutierrez et al., 1994; Nusser et al., 1995). However, to date there has been no clear physiological demonstration of activating distal dendritic GABAergic synapses on granule cells. These synapses may have different physiological properties from those present on the soma. Furthermore, synaptic events generated at different locations on granule cells may be distorted by cable filtering to different degrees, but as the detailed electrotonic structure of granule cells is not yet completely understood, it is difficult to ascertain what impact this will have on the effectiveness of distal inhibitory synapses.

In addition to the action potential–dependent release of GABA (Alger and Nicoll, 1980), inhibitory terminals are also capable of generating random inhibitory events in the absence of action potentials. The interevent intervals of such events are exponentially distributed (Otis et al., 1991; Otis and Mody, 1992; Soltesz and Mody, 1994), and they occur in most cells at relatively high frequencies (1–50 Hz). Although the precise role and mechanism of transmitter release associated with this type of tonic inhibitory synaptic transmission is not yet known, such inhibitory events

§Present address: Department of Neurology, University of California Los Angeles School of Medicine, Reed Neurological Research Center, Los Angeles, California 90095.

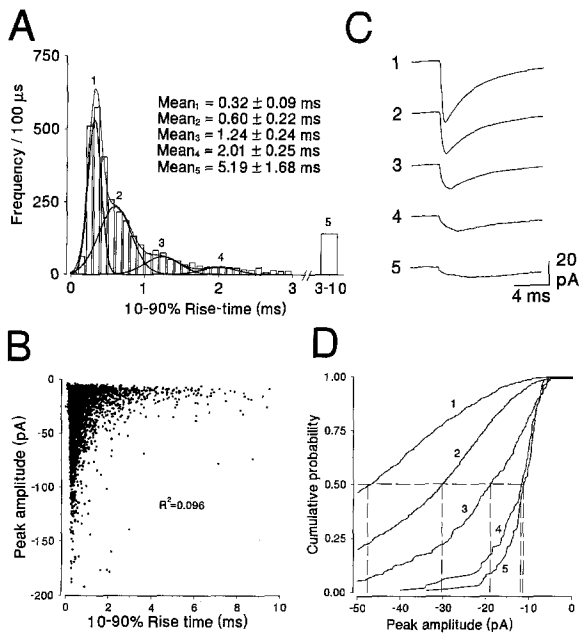

Figure 1. Evidence for the Effects of Cable Filtering on mIPSCs

(A) Distribution of the 10%–90% rise times of mIPSCs. The IPSCs in this figure were obtained by pooling 1100 events from each of three granule cells (total number of events, 3300). The recordings were selected on the basis of similar access resistances (8–10 MΩ). The rise times of mIPSCs range from 0.1–10 ms. Note that the distribution is skewed toward slower rise times, indicating that slower events are rarer. The distribution of mIPSCs with <3 ms rise times were fitted with four Gaussians, whereas those IPSCs with rise times 3–10 ms were pooled and represented as a separate bar on the right (there were too few events in this range to be reliably fitted with a single or multiple Gaussians). The mean and SD of each distribution are indicated.

(B) In contrast to the negative correlation present between the amplitude and rise times when populations of events are studied (see [C] and [D]), no such correlation can be found when individual mIPSCs are examined.

(C) Averages of mIPSCs obtained by selecting events with 10%–90% rise times within 1 SD around each of the five means shown in (A). This resulted in five nonoverlapping populations. This figure shows the averages of mIPSCs belonging to the five populations of events. Note that populations of miniature events with distinct and progressively slower rise times show progressively smaller amplitudes.

(D) Cumulative amplitude distributions for the five subpopulations shown in (A) and (B). Note that though fast events (population 1, for example) cover the whole range of amplitudes (larger events are to the left since they represent progressively more negative peak currents), slow events (e.g., population 5) are restricted to being small.

occurring at high frequencies are likely to be sufficient to exert a strong influence on the output of the cell. Removal of extracellular Ca^{2+} or addition of Ca^{2+} channel antagonists do not abolish miniature inhibitory postsynaptic currents (mIPSCs; Collingridge et al., 1984; Otis et al., 1991; Scanziani et al., 1992; Llano and Gerschenfeld, 1993), indicating that these events are independent of Ca^{2+} entry into the terminals. It is possible that spontaneous Ca^{2+} release from intracellular stores of inhibitory terminals is responsible for the generation of mIPSCs. Differences in the Ca^{2+}-handling mechanisms between terminals belonging to distinct interneuron types may therefore result in differences in action potential–independent GABA release. Different interneurons frequently express different Ca^{2+}-binding proteins (Katsumaru et al., 1988; Celio, 1990; Gulyás et al., 1991; Kawaguchi and Kubota, 1993). Inhibitory cells that synapse on the proximal parts of granule cells, the axo-axonic and basket cells, are all immunoreactive for parvalbumin, whereas cells that terminate in the dendritic layers are immunopositive for other Ca^{+}-binding proteins, such as calretinin and calbindin (Celio, 1990). In addition, it has been reported that inhibitory terminals on dendrites are smaller and contain mitochondria much less frequently than somatic terminals (Miles et al., 1995), suggesting that inhibitory terminals on different parts of a given neuron may have different capacities for handling Ca^{2+} and thus generating spontaneous GABA release.

In this study, we used whole-cell patch-clamp recordings and computational modeling to establish the site of origin of mIPSCs. This issue is fundamental to our understanding of how neuronal inhibition operates in cortical circuits. We find that action potential–independent random mIPSCs are restricted to GABAergic synapses situated on proximal parts of granule cells.

Results

mIPSCs Are Variable in Amplitude and Kinetics

One of the characteristic features of the amplitude and rise time distributions of spontaneously occurring IPSCs in all central neurons, recorded in the presence of glutamate receptor antagonists D-2-amino-5-phosphonovaleric acid (APV) and 6-cyano-7-nitroquinoxaline-2,3-dione (CNQX), is that they are skewed toward larger amplitudes and rise times (Figure 1A; see Figure 2A; Edwards et al., 1990; Doze et al., 1991; Otis and Mody, 1992). Such skewed amplitude and rise time distributions are found even when all action potential–dependent spontaneous IPSCs are blocked by the Na^{+} channel blocker tetrodotoxin (TTX; Edwards et al., 1990; Otis et al., 1991; Cohen et al., 1992; Otis and Mody, 1992; De Koninck and Mody, 1994). In granule cells of the dentate gyrus, for example, the 10%–90% rise times of the TTX-resistant mIPSCs range from 0.1 to 10 ms (Figure 1). Since all of these mIPSCs are blocked by the $GABA_A$ receptor antagonist bicuculline (25 µM; n = 3), they all result from the activation of $GABA_A$ receptors. The skewed amplitude and rise time distributions may be due to electrotonic filtering of the synaptic currents from different positions along the dendritic tree, from the possible presence of unequal numbers of $GABA_A$ receptors with various subunit compositions and kinetic properties at different synapses on the same cell, or both (De Koninck and Mody, 1994).

Clearly, synaptic currents with identical kinetics at their site of origin would be attenuated in their amplitudes and slowed in their rise times by varying degrees depending on how far the synapses are located from the site of recording, generally the soma (Rall, 1977; Spruston et al., 1993). Most studies, however, have concluded that electrotonic filtering does not significantly affect the measured distribution of spontaneous PSCs because they do not show a strong negative correlation between rise time and amplitude (Staley and Mody, 1991; Llano and Gerschenfeld,

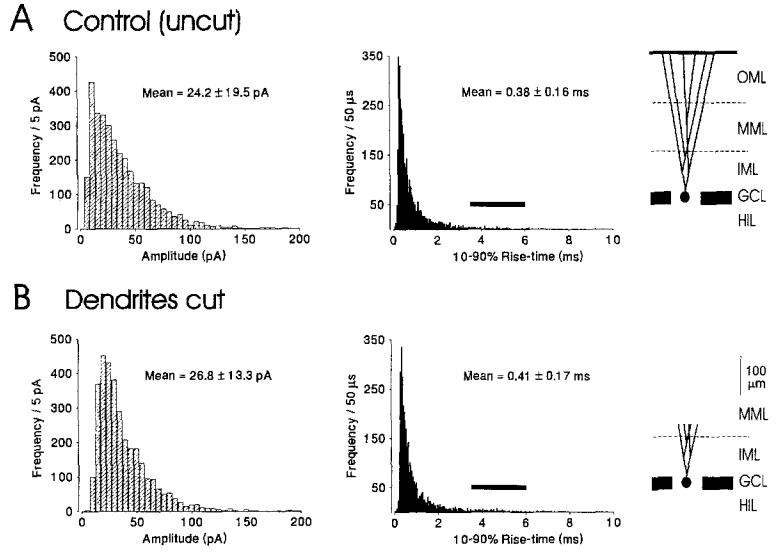

Figure 2. Lack of Effect of the Removal of the Bulk of the Dendritic Tree on mIPSCs

(A and B) Amplitude (left) and rise time distributions obtained from three control and three dendrotomized granule cells (each distribution has been obtained from 3300 mIPSCs, i.e., 1100 from each cell; all cells were recorded with similar access resistances of 8–10 MΩ). Note that there are no significant changes in the distributions nor in the mean amplitudes and mean rise times of the events. The schematic drawings on the right indicate the level at which dendrotomy was carried out. Note also that slow events with rise times >3 ms (marked by a horizontal bar in the middle panel) could readily be seen in neurons with amputated dendrites with a low frequency similar to that seen in control cells.

1993; Ulrich and Lüscher, 1993); this is also the case for granule cell mIPSCs (Figure 1B). However, simulations show that as these parameters change with electrotonic distance at drastically different rates (Spruston et al., 1993; D. K. Smetters and S. B. Nelson, 1994, Soc. Neurosci. Abstr.), there should be no simple linear relationship between them; therefore, the lack of a negative correlation cannot be taken as evidence for the absence of cable filtering (D. K. Smetters and S. B. Nelson, 1994, Soc. Neurosci. Abstr.; Smetters and Nelson, 1995). Additionally, any variability in underlying synaptic current amplitude or kinetics will mask the true relationship between these two parameters. Even though the relationship between these two parameters is not linear, in the presence of cable filtering, slow events should show a tendency to be smaller. This holds true for the mIPSCs recorded in dentate gyrus granule cells. Whereas fast events cover the whole range of amplitudes, slow events are restricted to being very small; similarly, the largest events tend to have very rapid rise times (Figure 1B). We have examined this in more detail by dividing the population of mIPSCs into nonoverlapping subpopulations with increasingly slower rise times (Figures 1C and 1D). We divided mIPSCs arbitrarily into five such subpopulations by fitting four Gaussians onto the distribution of 10%–90% rise times, whereas the fifth population (which contained too few events to be reliably fitted) was lumped together from events with 3–10 ms rise times (see legend to Figure 1 for details). Averages (Figure 1C) and cumulative amplitude distributions (Figure 1D) for these subpopulations show that when populations of IPSCs were studied, slower events tended to be smaller and larger ones faster, consistent with a role for cable filtering in shaping these events.

If cable filtering is responsible at least in part for the varied kinetics of mIPSCs, some mIPSCs must be generated at a distance from the somatic recording site. However, because neither the underlying synaptic kinetics nor the degree by which individual miniature events are distorted by electrotonic filtering are known, the exact site of generation of each event cannot be predicted. Consequently, from these data alone, it is not possible to estimate the proportion of mIPSCs generated at proximal versus distal sites.

Removal of Distal Dendrites Does Not Change the Amplitude or Kinetics of mIPSCs

One way to test whether inhibitory terminals situated distally generate spontaneous mIPSCs is to study the effects of the removal of these inputs on mIPSC amplitude and rise time distributions and their frequency. To achieve this, we surgically removed a large part of the dendritic tree. To avoid excitotoxic damage, dendrotomy was carried out in a neuroprotective medium (Soltesz and Mody, 1995), and mIPSCs were recorded from dendrotomized granule cells (n = 6). Removal of the bulk (>50%) of the dendritic tree with a cut made at the outer edge of the inner molecular layer (see Figure 2B, right) did not alter the amplitude and rise time distributions of mIPSCs (Figure 2; Kolmogorov-Smirnov test based on cumulative distributions, $p > .05$), nor did it change significantly the mean amplitude, rise time (Figure 2), or frequency (interevent intervals: control, 273 ± 64 ms, n = 6; dendrotomized, 325 ± 49, n = 6) of events.

This result suggests strongly that the mIPSCs we recorded under control conditions originated preferentially from proximal sites. However, it does not necessarily imply that terminals on dendrites do not generate mIPSCs. First, it is possible that in our preparation distal inhibitory terminals were not functional and could not release GABA. Second, distal mIPSCs may occur at relatively high frequencies, but attenuation by electrotonic filtering may render them undetectable at the soma.

Distal Inhibitory Terminals Are Capable of Releasing GABA and the Events They Generate Are Slow and Small

We obtained evidence for functional GABA synapses on distal dendrites by minimal stimulation of single GABAer-

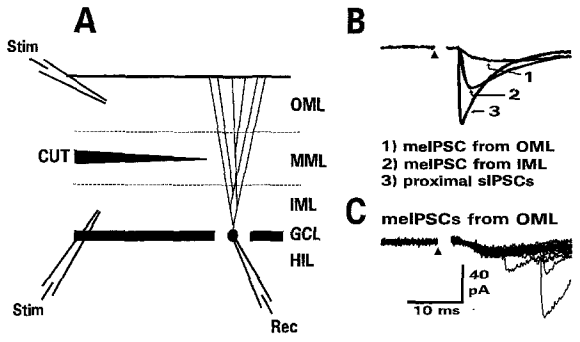

Figure 3. Effects of Cable Filtering on Minimally Evoked IPSCs

(A) Schematic drawing shows the experimental arrangement. A granule cell was recorded at the level of its soma, and a stimulating electrode was positioned either in the outer or the inner third of the molecular layer. A cut made parallel to the granule cell layer halfway in the molecular layer ensured that fibers stimulated distally did not branch onto the proximal dendritic tree.

(B) Minimally evoked IPSCs (mIPSCs) from the outer molecular layer showed slow rise times and small amplitudes (trace 1) when compared with those evoked from the IML (trace 2) or to the fastest spontaneous IPSCs (sIPSCs; trace 3). These fast sIPSCs with 10%–90% rise times <0.34 ms are the least affected by cable filtering and are likely to originate from somatic (proximal) sites. In addition, it has been shown that their kinetics are identical to those IPSCs that are evoked by minimal stimulation directly in the granule cell layer. For each case, the best fit currents (shown superimposed on the averages of IPSCs) were obtained using a single exponential rise and a single exponential decay function.

(C) An example of IPSCs evoked by minimal stimulation distally. Note the presence of fast, spontaneous IPSCs. Failures have been omitted for clarity.

HIL, hilus; GCL, granule cell layer; IML, MML, and OML, inner, middle, and outer molecular layer, respectively.

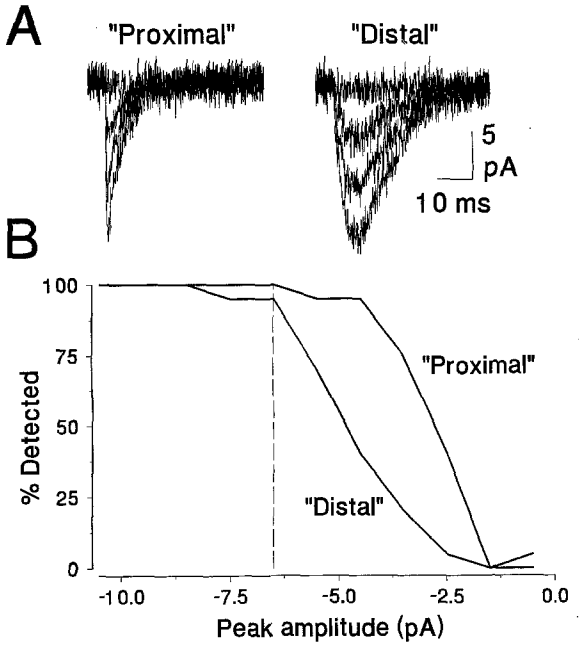

Figure 4. Detectability of mIPSCs of Varying Amplitudes and Kinetics

(A) Examples of simulated mIPSCs of varying amplitudes (−0.5 to −19.5 pA) and kinetics (fast [Proximal] and slow [Distal]; see text for details) used to test the sensitivity of the detector. Simulated mIPSCs are embedded in Gaussian noise of SD = 1.6 pA and filtered at 3 kHz.

(B) Percentage of events successfully detected in each kinetic class as a function of peak amplitude. More than 90% of the fast and slow events with amplitudes over 6.5 pA are detected.

gic fibers (Lambert and Wilson, 1993), in artificial cerebrospinal fluid (ACSF) containing APV and CNQX (without TTX). First, minimal stimulation was applied in the outer molecular layer (Figure 3A). To minimize the possibility of fibers crossing laminar boundaries, a cut was made at midlevel, parallel to the cell body layer. The cut ended as close as possible to the recorded cell (Figure 3A). As shown in Figures 3B and 3C, IPSCs could be easily evoked from the level of the distal dendrites, demonstrating the presence of functionally intact distal inhibitory terminals and synapses. Next, we compared the IPSCs obtained by minimal stimulation of single GABAergic fibers in the outer molecular layer with those from the inner molecular layer, as well as with the fastest of the spontaneously occurring events (10%–90% rise times, <0.34 ms) recorded from the same cells. Presumably, such fast events were the least affected by cable filtering and therefore are the most likely to originate from somatic (i.e., the most proximal) sites. Furthermore, their kinetics are identical to those IPSCs evoked by minimal stimulation directly in the cell body layer (Edwards et al., 1990; Lambert and Wilson, 1993; Mody et al., 1994). As is shown in Figure 3B, it was clear that the further away from the soma the IPSCs were generated, the smaller and slower they became. Thus, the smallest (peak amplitude, −13.0 ± 1.7 pA) and slowest (10%–90% rise time, 5.0 ± 0.7 ms; range, 3.6–6.5 ms; n = 6) events were evoked by minimal stimulation in the outer molecular layer (Figure 3C; 10%–90% rise time of the responses from the inner molecular layer, 0.79 ± 0.2 ms). These results clearly show that functional GABAergic terminals and synapses are present on distal dendrites of granule cells. In addition, the findings also demonstrate that the amplitude and kinetics of IPSCs originating distally but recorded at the soma are different from those of proximal IPSCs. Such differences in IPSC amplitude and kinetics are consistent with an effect of cable filtering in shaping the synaptic responses measured at the soma.

Are Slow Distal mIPSCs Missed by the Event Detector?

An important consideration in estimating the number of very slow, small, presumably distal events is our ability to detect them. Perhaps there is a large population of these slow events, but our detector only allows us to discern the largest ones. This may explain why the slower events represent a progressively smaller percentage of the total population of mIPSCs (see Figure 1A). To determine the sensitivity of our method for detecting mIPSCs, we tested its ability to detect simulated events embedded in noise. We generated events of varying amplitudes in different kinetic classes according to equation 1 (see Experimental Procedures), "proximal" (τ_R = 0.146 ms, τ_D = 4.385 ms; obtained by fitting the average of the 25% fastest mIPSCs

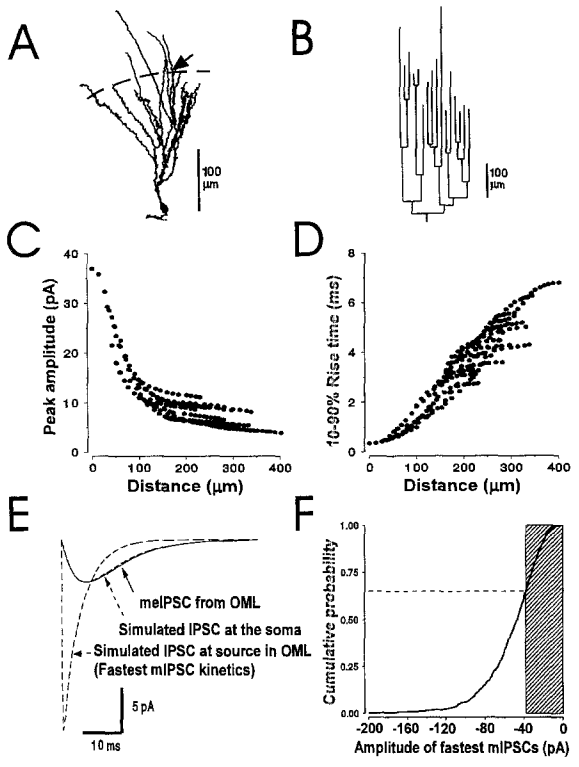

Figure 5. Compartmental Simulations of mIPSCs and Prediction of the Percentage of Distal Events That Should Be Detectable

(A and B) Camera lucida image of the reconstructed granule cell used in the simulations (A) and its corresponding dendrogram (B). The cell was filled with biocytin in vivo during the course of another study (Soltesz and Deschênes, 1993). In (A), the dashed line indicates the region in which we evoked mIPSCs in the outer molecular layer (Figure 3), and the arrow shows the position of the synapse used in the simulations shown in (E).

(C and D) Distributions of simulated mIPSC amplitude and 10%–90% rise times with distance from the granule cell layer (R_m = 40,000 Ωcm², R_i = 100 Ωcm, R_s = 7 MΩ, g = 0.75 nS). The measured amplitude decays rapidly over the first 50–100 µm and then plateaus at approximately 10 pA. Rise times show a linear relationship with distance and cover the same range as both the recorded minimally evoked IPSCs and the slowest mIPSCs.

(E) Simulated mIPSCs show similar kinetics to the evoked IPSCs using input kinetics measured at the soma. Trace labeled "Simulated IPSC at source in OML" is a simulated mIPSC measured at the soma for an input synaptic current with the average kinetics of the fastest, most probably somatic mIPSCs (parameters same as in [C]). In trace labeled "Simulated IPSC at the soma," the same input is placed onto a dendrite 250 µm (indicated by the dashed line in [A]; the position of the synapse is indicated by an arrow) from the granule cell layer (i.e., in the middle of the outer molecular layer, in the region where we evoked minimal IPSCs), and the response measured at the soma. The overlying trace is the fit to an actual evoked IPSC stimulated at a site 250 µm from the granule cell layer, indicating both the plausibility of the model and, more importantly, that cable filtering alone is sufficient to generate a very good match to the slow kinetics of both the distal minimally evoked IPSCs and the slowest mIPSCs (also see [C] and [D]), without requiring different distal synaptic kinetics or temporal dispersion of release.

(F) Assuming that distal mIPSCs have the same underlying distribution of amplitudes at source as the "somatic" mIPSCs (the fastest events, population 1 in Figure 1A), we estimated from the model that we should be able to detect 60% of the distal events (see text for details). The shaded region on the cumulative probability plot shows the proportion of the events that would remain undetectable if generated in the distal dendrites.

with the sum of a single exponential rise and single exponential decay) and "distal" (τ_R = 6.242 ms, τ_D = 6.422 ms; obtained by fitting the IPSCs evoked by minimal stimulation of the outer molecular layer; see Figure 3C). Simulated mIPSCs were embedded in Gaussian noise of SD = 1.6 pA, corresponding to the high end of the experimental range, and filtered at 3 kHz (Figure 4A). These simulated data files were then run through the detector, and the percentage of each event category that was successfully detected was measured. We successfully detected >90% of the proximal and distal events with amplitudes of at least 6.5 pA (Figure 4B). This indicates that we should detect almost all distal events with amplitudes ⩾ 6.5 pA and kinetics similar to or faster than the slow minimally evoked events. In fact, even in the extreme case of ultraslow simulated events (τ_R = 11.0 ms, τ_D = 14.0 ms; although such IPSCs were never observed experimentally), we were still able to detect >90% of the events with amplitudes >9.5pA.

Computational Modeling of the Influence of Synaptic Location on IPSC Amplitude and Kinetics in Granule Cells

Two important questions arise. First, what fraction of the distally generated mIPSCs should we observe with our measured detection threshold of 6.5 pA? Based on the amplitudes of the minimally evoked IPSCs from the outer molecular layer (−13.0 ± 1.7 pA), which were well above our detection threshold, we would expect that mIPSCs originating 250 µm from the granule cell layer (i.e., the middle of the outer molecular layer) would be easily detectable. However, we do not know the number of terminals originating from an individual interneuron that synapse onto the dendrites of a single granule cell. Therefore, it is possible that the IPSCs evoked by minimal stimulation from distal sites are larger than distal mIPSCs, because the evoked IPSCs may be elicited by several terminals belonging to the same axon. The second question is, are cable filtering and synaptic location sufficient to explain the amplitudes and kinetics of the distally generated IPSCs. It could be that the underlying channel kinetics at distal synapses (which arise from a different population of inhibitory interneurons than the proximal ones do) are slower at source than those seen at the soma, or that the minimally evoked IPSCs are made up of multiple small quanta released asynchronously, thus extending the time course of the resulting synaptic current.

To answer these questions, we have turned to compartmental modeling of a typical granule cell (Figures 5A and 5B; see Experimental Procedures for details). We estimated the underlying kinetics of the GABAergic synaptic current by selecting the 25% fastest of the mIPSCs (those most likely to be somatic) and fitting them with equation 1. We then placed a synapse with these kinetics onto each compartment of the granule cell model and obtained the amplitude and kinetics of the currents that would be recorded at the soma. The distribution of response parameters with increasing distance from the granule cell layer is shown in Figures 5C and 5D. Peak amplitude decreases

very rapidly as the synapse is moved away from the soma, and then plateaus after 50–100 μm, showing only slight further decline. The 10%–90% rise time increases basically linearly with increasing distance from the soma.

Simulated 10%–90% rise times cover a very similar range to those seen in mIPSCs and minimally evoked IPSCs. This implies that cable filtering alone is sufficient to account for the slow kinetics and small amplitudes of the minimally evoked IPSCs from the outer molecular layer. Furthermore, the slow, small mIPSCs could be generated by synaptic events with the same kinetics as the putative somatic mIPSCs but placed onto a distal site (also see Figure 5E). Figure 5C also shows that even in the first 100 μm of the most proximal region of the dendrites (the region that remains intact in the cut granule cells of Figure 2), there is still a significant effect of cable filtering on both mIPSC amplitude and rise time.

To test the validity of our granule cell model, we placed a synaptic current with kinetics of the fastest, most likely somatic IPSCs in the middle of the outer molecular layer (i.e., 250 μm away, indicated by the dashed line in Figure 5A; the position of the synapse is indicated by an arrow) in the region where we evoked minimal IPSCs. As it is shown in Figure 5E, the modeled response of this IPSC as seen at the somatic recording site perfectly matched the kinetics of the IPSC obtained by minimal stimulation. The conductance of the simulated distal input was 0.745 nS, which is not considerably different from the mean conductance of the putative somatic mIPSCs (0.83 nS, assuming a synaptic reversal potential of 0 mV; Figure 5F) or the fastest, putatively somatic, spontaneous IPSCs recorded in the cell used for minimal stimulation in Figure 3B (1.18 nS, events recorded in the absence of TTX). This result shows that our granule cell model describes well the cable properties of these neurons, and it also indicates that the kinetics of distal minimally evoked IPSCs at source are comparable to those of the presumed somatic mIPSCs.

Percent of mIPSCs from Distal Sites That Should Be Detectable

For each synaptic site, we have estimated the mIPSC conductance at this site necessary to generate a 6.5 pA mIPSC at the soma (the threshold mIPSC for this site). We then calculated what the amplitude of this mIPSC would have been if it had been placed directly onto the soma (the threshold somatic amplitude). We assumed that the distal synapses show the same distribution of mIPSC peak conductances as the somatic mIPSCs. Next, we estimated how many of those events we should be able to detect by looking at where the threshold somatic amplitude for each site fell on the distribution of somatic mIPSC peak amplitudes (generated by selecting the fastest rising 25% of the mIPSCs; their cumulative amplitude distribution is shown in Figure 5F). To take into account the variance among different dendrites, we averaged these threshold mIPSC amplitudes from sites in 20 μm bins from the soma. Given the parameters used in Figures 5C–5E, the threshold somatic amplitude for those points from 240 to 260 μm from the soma (the region stimulated to obtain minimally evoked IPSCs) would be 38 pA (see also Figure 5C). Of the putative somatic mIPSCs, 60% are larger than 38 pA (Figure 5F). If these distal synaptic sites draw their mIPSC amplitudes from a similar distribution as the somatic events do (which is suggested by the good match between simulated distal and slow IPSC in Figure 5E), then we must be detecting 60% of the events generated 250 μm away from the soma, as shown by the hatched region in Figure 5F. Naturally, we would detect a larger fraction of events generated more proximally than 250 μm from the soma.

We have also explored the effects of changing the passive parameters of the model (data not shown; see Experimental Procedures for details). Increasing R_m several-fold only increases the percentage of distal events we should record while at the same time slowing their kinetics even further (Spruston et al., 1993; Jonas et al., 1993; Major et al., 1994); this would indicate that the bulk of events we see are generated even more proximally than postulated here. Increasing R_i to 200 or 300 Ωcm, as has been suggested by recent studies (Major et al., 1994), however, does significantly increase the attenuation of distal events, and hence lowers the fraction of those events we can detect. However, increasing R_i also slows event kinetics, meaning that events closer to the soma (whose amplitudes are less attenuated) will generate events with 3–6 ms rise times. These two effects together indicate that we should still see a much larger number of events with long rise times than we do if they were being generated at dendritic sites at the same rate as they are somatically.

Taken together, these results indicate that distal mIPSCs should have rise times comparable to those of the minimally evoked IPSCs from the outer molecular layer (3.5–6 ms) because they would be subjected to the same amount of dendritic filtering. Since, as described above, our detector can detect 60% of the mIPSCs originating distally, there should be a large percentage of the total number of mIPSCs with 10%–90% rise times slower than 3 ms. However, there were very few (3%) mIPSCs with rise times in this range (see Figure 1A and Figure 2A). This observation is consistent with the proximal origin of mIPSCs, as suggested by the experiments involving removal of dendrites.

Discussion

Of all GABAergic synapses in the dentate gyrus, 75% are located in the layer of granule cell dendrites (Halasy and Somogyi, 1993a). These terminals originate from distinct interneuron types, each of which innervate particular parts of the dendritic tree (Han et al., 1993; Buhl et al., 1994a, 1994b). The anatomical segregation of the inhibitory inputs to granule cells suggests heterogeneity in the functional roles of proximal versus distal inhibitory inputs, and possibly differences between the proximal versus distal inhibitory terminals themselves. In addition to the anatomical differences, including bouton size and mitochondrial content (Miles et al., 1995), there are also pharmacological differences between somatic and dendritic inhibitory terminals. For example, in the CA3 region, somatic and den-

dritic terminals show different degrees of regulation of GABA release by presynaptic $GABA_B$ receptors (Lambert and Wilson, 1993).

One powerful technique for exploring synaptic function is the study of spontaneously generated synaptic events (Mody et al., 1994). However, electrophysiological recordings of spontaneous IPSCs do not reveal the location of the GABAergic synapses from which they arise, making it difficult to study the relationship between synaptic location and function. Investigations aimed at revealing the site of origin of spontaneous IPSCs are hampered by the lack of knowledge of the extent to which synaptic currents are altered by electrotonic filtering in granule cells. In addition, the 11 different $GABA_A$ receptor subunits known to be expressed by granule cells (Schoch et al., 1985; Richards et al., 1987; Houser et al., 1988; Zimprich et al., 1991; Wisden et al., 1992; Turner et al., 1993; Gao and Fritschy, 1994; Nusser et al., 1995) may be distributed differentially at synapses, forming receptor-channel pentamers with distinct kinetic properties, which would further complicate any study of the site of origin of mIPSCs. For example, in CA1 pyramids, Pearce (1993) has shown the existence of distinct fast somatic and slower dendritic $GABA_A$ IPSCs and suggested that different $GABA_A$ receptors may be activated by these two classes of inhibitory inputs, as cable filtering could not completely account for the slow decay kinetics of the dendritic IPSCs. But, as it has been shown to be the case for excitatory currents in pyramidal cells, electrotonic filtering can still drastically influence synaptic signals (Williams and Johnston, 1991; Jonas et al., 1993).

We have demonstrated that cable filtering can play a role in shaping the kinetics and amplitudes of the different mIPSCs observable in a single neuron. Traditionally, the impact of cable filtering is assessed by measuring the degree of correlation between the rise times and amplitudes of individual mIPSCs. Using this procedure, no strong negative correlation can be found between mIPSC rise times and amplitudes; this is also the case for excitatory spontaneous events in a variety of cell types (Staley and Mody, 1991; Stern et al., 1992; McBain and Dingledine, 1992, 1993; Ulrich and Lüscher, 1993; Jonas et al., 1993). In spite of this lack of a linear negative correlation, populations of miniature events with distinct and progressively slower rise times do show progressively smaller amplitudes (see Figure 1D), and this is true regardless of the precise algorithm used to sort mIPSCs into subpopulations. An alternative explanation of this result is that the GABAergic synapses on granule cells vary widely in their kinetics, and additionally, those with slow kinetics are somehow restricted to having a smaller number of receptor channels and hence a lower total conductance. However, this is unlikely, as a similar relationship between amplitude and rise time (which can be simply derived from the appearance of the rise time versus amplitude plot [Figure 1B], without the more complicated analysis shown here) can be seen across a wide variety of cell and synapse types (Staley and Mody, 1991; Stern et al., 1992; McBain and Dingledine, 1992, 1993; Ulrich and Lüscher, 1993; Llano and Gerschenfeld, 1993; Jonas et al., 1993). Then, this result is consistent with mIPSC kinetics and amplitudes being altered by cable filtering. Thus, in all likelihood, some mIPSCs are generated at a distance from the soma.

Yet, these results do not reveal just how far from the soma the most distal mIPSCs are being generated. We tested this by removing the bulk of the dendritic tree. When the amputation of dendrites is carried out in neuroprotective media (Soltesz and Mody, 1995), the neurons survive, and the kinetics of the mIPSCs are not affected. Granule cells are ideally suited for such investigations, since they are tightly packed in a cell layer and, in the rat, they are devoid of basal dendrites. A cut made at the outer edge of the inner molecular layer removes more than half of the total dendritic tree. Since the cut is parallel to the granule cell layer and involves half of the dentate gyrus (the other half normally serves as control), there is no possibility for any granule cell on the dendrotomized side to escape amputation of its dendrites. Recordings from such dendrotomized neurons showed unequivocally that there was no change in the amplitude and rise time distributions. The mean amplitude, rise time, and frequency of the mIPSCs in dendrotomized cells were also comparable to those in controls. Thus, mIPSCs recordable at the soma must all be generated more proximally than the outer edge of the inner molecular layer.

Minimal stimulation in the distal dendritic layer clearly dismissed the possibility that inhibitory synapses situated on distal dendrites are unable to release GABA onto functional receptors. In addition, we found it no more difficult to evoke IPSCs minimally in the outer molecular layer as in the inner molecular layer, indicating that there was no difference in the availability of proximally and distally projecting axons after slicing. This is consistent with anatomical studies showing that proximally projecting inhibitory axons (i.e., from basket and axo-axonic cells) cover a large area (Han et al., 1993) and are as likely to be cut in the slicing procedure as are the axons of interneurons innervating distal dendrites. Furthermore, experiments with minimal stimulation in the proximal and distal dendritic layers provided direct evidence for the extent of cable filtering of GABAergic IPSCs. As has been described before, the narrow stimulus intensity threshold, the fixed latency, and the kinetics of the minimally evoked IPSCs are all consistent with the activation of single fibers (Edwards et al., 1990; Lambert and Wilson, 1993). As the site of minimal stimulation was moved farther out along the dendritic axis of the cell, the amplitude and rise time of the resulting evoked IPSCs changed in a manner consistent with the effect of electrotonic filtering. Importantly, simulations showed that the kinetics of the distally evoked IPSCs at source were likely to be very similar to the kinetics of the somatic spontaneous IPSCs (Figures 5C–5E). According to this finding, there are no major systematic differences between the kinetic properties of $GABA_A$ receptors in the outer molecular layer versus those located on the soma, although subtle differences may occur. In addition, the near-perfect match shown in Figure 5E between the distally evoked IPSC and the somatic recording of the distally positioned fastest spontaneously occurring IPSCs in the model also provided an independent check on the validity

of the parameters used in the compartmental model, since it is extremely unlikely to have come about only by chance.

Since the model proved to be a realistic representation of granule cells, we could use it to estimate the percentage of the distal mIPSCs that we should detect if they occurred with the same amplitude distribution as the putative somatic mIPSCs (see below; Figure 5D). We concluded that more than 60% of these spontaneous dendritic events should be detectable in our system. However, the population of events with >3 ms rise times (i.e., those potentially originating in the outer molecular layer) comprised only a very small fraction of the total population of mIPSCs, approximately 3%. In fact, as shown by the experiments involving the amputation of dendrites, even this small population of slow mIPSCs were generated at sites closer than the middle molecular layer.

The simulations also showed that even those mIPSCs generated close to the soma would have their amplitudes drastically attenuated by cable filtering (Figure 5C), and the rise times of events generated within the inner molecular layer could be slowed to as long as 3 ms (Figure 5D). Although this paper does not address whether the effects of cable filtering or those of different $GABA_A$ receptor subunit assemblies with distinct kinetics are the more important factors underlying the generation of nonuniform mIPSCs in a single cell, it is interesting to note that the considerable effects of cable filtering acting on IPSCs generated within the first 100 μm from the cell body can, in principle, explain a large part of the mIPSC variability in both control and dendrotomized cells. The presence in both control and dendrotomized neurons of a small percentage of very slow (>3 ms) events, together with the absence of such events generated within 150 μm of the soma in the simulations (Figure 5), may suggest the existence of a small number of proximal synapses with distinct $GABA_A$ receptor subunit composition and kinetics.

The apparent lack of major differences between the somatic versus distal dendritic $GABA_A$ receptors allowed us to make assumptions about the possible distributions of distal IPSC amplitudes from the distribution of somatic event amplitudes, as we did when we estimated the percentage of distal mIPSCs (Figure 5F). We cannot rule out the possibility that, at distal inhibitory terminals, the number of functional $GABA_A$ receptors per synapse may be lower, and thus the distal events may be of significantly smaller amplitude at source. However, the immunostaining for $GABA_A$ receptor subunits studied so far appears to be homogeneous in the dendritic layer (Schoch et al., 1985; Richards et al., 1987; Houser et al., 1988; Zimprich et al., 1991; Turner et al., 1993; Gao and Fritschy, 1994; Nusser et al., 1995). But even if the percentage of distal mIPSCs that we could see was lower than the 60% estimated here because of amplitude differences at source, we should observe many more than 3% of the total number of events with >3 ms rise times. Therefore, distal terminals cannot substantially contribute to the generation of mIPSCs. We conclude that the frequent and random mIPSCs typically recorded are predominantly generated at proximal synapses. If there was an undetectable population of very small distal mIPSCs, given their electrotonic invisibility at the soma, these events would be expected to have a limited impact on the output of the cell.

At present, we can only speculate why only proximal inhibitory terminals are capable of releasing GABA independently of action potentials. After all, the dendritic synapses appeared fully functional in our preparation, since minimal stimulation could evoke IPSCs from the outer molecular layer. It seems likely that the anatomical differences between somatic versus dendritic terminals (Miles et al., 1995) may underlie some functional difference between them. For example, local application of sucrose in the granule cell layer results in a large increase in the frequency of mIPSCs with a very short latency (1–3 s), whereas sucrose application in the outer molecular layer in the same cell causes only a small and rather delayed (>10 s) increase (see, for example, Figure 5 in Mody et al., 1994). Although the precise mechanism of action of hyperosmotic solutions on transmitter release has not yet been determined, the failure of sucrose to increase GABA release from distal terminals may also be associated with the smaller size or other anatomical differences between dendritic and somatic GABAergic terminals.

Functional Implications for Cortical Inhibition

Our findings reveal that the tonic, action potential–independent GABA release takes place preferentially, or perhaps exclusively, at sites close to the action potential initiation site in granule cells. Based on our data, the random tonic inhibition is primarily a result of miniature events generated by the neurons with proximal termination zones, most likely basket and axo-axonic cells. A functional division of labor may thus exist between subclasses of inhibitory cells that innervate proximal versus distal regions of principal neurons, corresponding to the differerent roles that have been previously suggested for somatic and dendritic inhibition (Vu and Krasne, 1992; Bush and Sejnowski, 1994; Koch et al., 1982, 1983). The restricted nature of tonic, action potential–independent GABAergic inhibition is likely to play an important role in regulating the input–output relations of central neurons.

Experimental Procedures

Preparation of Slices

The preparation of slices was done as previously described (Otis and Mody, 1992; Staley et al., 1992). In brief, adult (60–120 days old; 250–350 g) male Wistar rats were decapitated under pentobarbital sodium anesthesia (75 mg/kg intraperitoneal) and the brains removed. The brain was cooled in 4°C ACSF composed of 126 mM NaCl, 2.5 mM KCl, 26 mM $NaHCO_3$, 2 mM $CaCl_2$, 2 $MgCl_2$, 1.25 mM NaH_2PO_4, and 10 mM glucose. Horizontal whole-brain slices (400 μm thick; Staley and Mody, 1991) were prepared using a vibratome tissue sectioner (Lancer Series 1000). The brain slices were sagitally bisected into two hemispheric components and submerged in a temporary storage chamber.

For the experiments involving the amputation of dendrites (Soltesz and Mody, 1995), the slices were preincubated at 32°C submerged in a temporary storage chamber in neuroprotective media containing 25 μM APV (Cambridge Research Biochemicals) and 10 μM CNQX (Tocris Neuramin). Following preincubation, a cut was made parallel to the granule cell layer at the level of the outer edge of the inner third of the molecular layer on one of the two sides (i.e., blades) of the

dentate gyrus (Soltesz and Mody, 1995). The distal part of the cut dendritic layer was removed. Both cut and uncut (control) slices were then transferred to a storage chamber, where they were kept in ACSF at 32°C for at least 90 min before recording.

Electrophysiology

Electrodes and Solutions

Patch electrodes were pulled from borosilicate (KG-33) glass capillary tubing (1.5 mm o.d.; Garner Glass) using a Narishige PP-83 two-stage electrode puller. The intracellular solution was made up in high performance liquid chromatography grade water (Omnisolve, EM Science, Gibbstown, NJ) and was composed of 135 mM CsCl, 2 mM $MgCl_2$, and 10 mM HEPES; the solution was buffered with CsOH to pH 7.2 and filtered through a 0.2 μm pore size filter (Nalgene). No exogenous Ca^{2+} buffers were used. Final osmolarity for all solutions ranged between 260–280 mOsm. All salts were obtained from Fluka.

Recordings

Whole-cell recordings were obtained blind (Blanton et al., 1989; Staley et al., 1992) with an Axopatch-200A amplifier (Axon Instruments) digitized at 88 kHz (Neurocorder, NeuroData) before being stored in PCM form on videotape. The ACSF contained 25 μM APV, 10 μM CNQX, and to record mIPSCs, 1 μM TTX (Calbiochem) was also added. Access resistances were <15 MΩ. Minimal stimulation was carried out as described previously (Edwards et al., 1990; Lambert and Wilson, 1993). In brief, patch pipettes filled with the extracellular medium were used to stimulate single fibers. The stimulating electrode was positioned at various distances from the granule cell layer (see Figure 3) and at least 300 μm away from the recorded cell. Low intensity stimuli elicited no response, but upon gradual increase in intensity, IPSCs were evoked in an all-or-none fashion. When the stimulus intensity was raised above threshold, the percentage of failures decreased but in most cases did not alter the kinetics of the responses. Such narrow threshold of stimuli indicates that the minimally evoked IPSCs probably result from the activation of single inhibitory fibers (Edwards et al., 1990; Lambert and Wilson, 1993). Statistical analyses (t test or F test) were performed using SPSS for Windows with a level of significance of $p \leq .05$. Data are presented as mean ± SEM (n = number of cells).

Analysis

Off-line, the recordings were filtered DC to 1–3 kHz (8-pole Bessel) before digitization at 20 kHz by computer (Data Translation DT 2821 A/D board in an Intel 486/66 MHz computer). The digitization and analysis were done using the Strathclyde Electrophysiology software (courtesy of J. Dempster). Detection of individual mIPSCs was done using a software trigger supplied by Dr. Dempster as part of the Strathclyde Electrophysiology software package. This detector is basically an amplitude-threshold based detector. A least squares Simplex–based algorithm was used to fit the ensemble average with the sum of two (one rising and one decaying) exponentials:

$$I(t) = -A \times e^{-\tau_R/t} + A \times e^{-\tau_D/t} \quad (1)$$

where I(t) is the mIPSC as a function of time (t), A is a constant, and τ_R and τ_D are the rise and decay time constants, respectively.

Simulations

Compartmental simulations were performed using a reconstructed dentate gyrus granule cell filled with biocytin in vivo during the course of another study (Soltesz and Deschênes, 1993), from an animal of similar age and size to those used in the current study. The cell was reconstructed in three dimensions using a Eutectics NTS reconstruction system from 80 μm sections (100 × objective, 1.3 nA); 10% shrinkage was assumed in the simulations presented here. Total dendritic extent in the Z direction was under 400 μm, so it was assumed that the complete cell would have been present in a coronal slice, and no additional cropping of the cell was performed. Simulations were performed using NEURON (courtesy M. Hines). The reconstructed cell was divided into compartments of less than 20 μm in length, and the presence of spines was corrected for by altering the values of R_m and C_m (Holmes, 1989). Spine densities and areas were taken from Desmond and Levy (1985) and were consistent with spine counts taken directly from the cell used here. We used several sets of passive cellular parameters chosen to be consistent with recent computational studies and the range of input resistances measured here (these included R_m = 40,000 Ωcm², R_i = 100 Ωcm, C_m = 1 μF/cm² [Spruston and Johnston, 1992]; R_m = 50,000 Ωcm², R_i = 200 Ωcm, C_m = 1 μF/cm² [Spruston et al., 1993]; R_m = 50,000 Ωcm², R_i = 300 Ωcm, C_m = 0.7 μF/cm² [Major et al., 1994]). Synaptic inputs were simulated as a difference of two exponentials according to equation 1. Kinetics for all synapses were taken from the fit to the average of the largest, fastest mIPSCs (those most likely to be purely somatic; τ_R = 0.146 ms, τ_D = 4.583 ms). The simulated cell was voltage clamped at −60 mV; in simulations shown here, an explicit series resistance of 7 MΩ (the average of the experimental values) was included. Electrode capacitance was not explicitly modeled. There is an additional potential source of error, owing to the fact that the Cl^--loaded granule cell dendrites may not rest at −60 mV, and therefore there may be a slight decrease in steady-state voltage and hence synaptic driving force with distance from the electrode. This was estimated to cause less than a 10% reduction in driving force, so it was considered negligible. The X, Y, and Z coordinates of each dendritic point were preserved in the simulation. These were used to calculate the distance of each simulated dendritic site from the midpoint of the cell body layer, taken as the centroid of the soma (the soma of this cell was in the middle of the cell body layer of the upper blade of the dentate gyrus).

Acknowledgments

We thank Dr D. Johnston for comments on the manuscript, Dr Y. De Koninck for writing the analysis programs and for stimulating discussions, Dr J. Yang for advice, Dr. M. Hines for NEURON, Dr J. Dempster for the Strathclyde Electrophysiology Software, and J. Gruneich for technical assistance. This work was supported by National Institute of Neurological Diseases and Stroke Grant NS-30549 to I. M. and a Howard Hughes Medical Institute predoctoral fellowship to D. K. S.

The costs of publication of this article were defrayed in part by the payment of page charges. This article must therefore be hereby marked *"advertisement"* in accordance with 18 USC Section 1734 solely to indicate this fact.

Received January 12, 1995; revised February 28, 1995.

References

Alger, B. E., and Nicoll, R. A. (1980). Spontaneous inhibitory postsynaptic potentials in hippocampus: mechanism for tonic inhibition. Brain Res. *200*, 195–200.

Benke, D., Mertens, S., Trzeciak, A., Gillessen, D., and Mohler, H. (1991). Identification and immunohistochemical mapping of $GABA_A$ receptor subtypes containing the subunit in the rat brain. FEBS Lett. *283*, 145–149.

Blanton, M. G., Lo Turco, J. J., and Kriegstein, A. R. (1989). Whole cell recording from neurons in slices of reptilian and mammalian cerebral cortex. J. Neurosci. Meth. *30*, 203–210.

Buhl, E. H., Halasy, K., and Somogyi, P. (1994a). Diverse sources of hippocampal unitary inhibitory postsynaptic potentials and the number of synaptic release sites. Nature *368*, 823–828.

Buhl, E. H., Han, Z. S., Lörinczi, Z., Stezhka, V. V., Karnup, S. V., and Somogyi, P. (1994b). Physiological properties of anatomically identified axo-axonic cells in the rat hippocampus. J. Neurophysiol. *71*, 1289–1307.

Bush, P. C., and Sejnowski, T. J. (1994). Effects of inhibition and dendritic saturation in simulated neocortical pyramidal cells. J. Neurophysiol. *71*, 2183–2193.

Celio, M. R. (1990). Calbindin D-28k and parvalbumin in the rat nervous system. Neuroscience *35*, 375–475.

Cohen, G. A., Doze, V. A., and Madison, D. V. (1992). Opioid inhibition of GABA release from presynaptic terminals of rat hippocampal interneurons. Neuron *9*, 325–335.

Collingridge, G. L., Gage, P. W., and Robertson, B. (1984). Inhibitory post-synaptic currents in rat hippocampal CA1 neurones. J. Physiol. *356*, 551–564.

De Koninck, Y., and Mody, I. (1994). Noise analysis of miniature IPSCs in adult rat brain slices: properties and modulation of synaptic $GABA_A$ receptor channels. J. Neurophysiol. *71*, 1318–1335.

Desmond, N. L., and Levy, W. B. (1985). Granule cell dendritic spine density in the rat hippocampus varies with spine shape and locations. Neurosci. Lett. *54*, 219–224.

Doze, V. A., Cohen, G. A., and Madison, D. V. (1991). Synaptic localization of adrenergic disinhibition in the rat hippocampus. Neuron *6*, 889–900.

Edwards, F. A., Konnerth, A., and Sakmann, B. (1990). Quantal analysis of inhibitory synaptic transmission in the dentate gyrus of rat hippocampal slices: a patch-clamp study. J. Physiol. *430*, 213–249.

Gao, B., and Fritschy, J. M. (1994). Selective allocation of $GABA_A$ receptors containing the α1 subunit to neurochemically distinct subpopulations of rat hippocampal interneurons. Eur. J. Neurosci. *6*, 837–853.

Gulyás, A. I., Tóth, K., Dános, P., and Freund, T. F. (1991). Subpopulations of GABAergic neurons containing parvalbumin, calbindin D28k, and cholecystokinin in the rat hippocampus. J. Comp. Neurol. *312*, 371–378.

Gutierrez, A., Kahn, Z. U., and De Blas, A. (1994). Immunocytochemical localization of gamma 2 short and gamma 2 long subunits of the $GABA_A$ receptor in the rat brain. J. Neurosci. *14*, 7168–7179.

Halasy, K., and Somogyi, P. (1993a). Distribution of GABAergic synapses and their targets in the dentate gyrus of rat: a quantitative immunoelectron microscopic analysis. J. Hirnforsch. *34*, 299–308.

Halasy, K., and Somogyi, P. (1993b). Subdivisions in the multiple GABAergic innervation of granule cells in the dentate gyrus of the rat hippocampus. Eur. J. Neurosci. *5*, 411–429.

Han, Z.-S., Buhl, E. H., Lörinczi, Z., and Somogyi, P. (1993). A high degree of spatial selectivity in the axonal and dendritic domains of physiologically identified local-circuit neurons in the dentate gyrus of the rat hippocampus. Eur. J. Neurosci. *5*, 395–410.

Holmes, W. R. (1989). The role of dendritic diameters in maximizing the effectiveness of synaptic inputs. Brain Res. *478*, 127–137.

Houser, C. R., Olsen, R. W., Richards, J. G., and Möhler, H. (1988). Immunohistochemical localization of benzodiazepine/$GABA_A$ receptors in the human hippocampal formation. J. Neurosci. *8*, 1370–1383.

Jonas, P., Major, G., and Sakmann, B. (1993). Quantal components of unitary EPSCs at the mossy fibre synapse on CA3 pyramidal cells of rat hippocampus. J. Physiol. *472*, 615–663.

Katsumaru, H., Kosaka, T., Heizmann, C. W., and Hama, K. (1988). Immunocytochemical study of GABAergic neurons containing the calcium-binding protein parvalbumin in the rat hippocampus. Exp. Brain Res. *72*, 347–362.

Kawaguchi, Y., and Kubota, Y. (1993). Correlation of physiological subgroupings of nonpyramidal cells with parvalbumin- and $calbindin_{D28K}$-immunoreactive neurons in layer V of rat frontal cortex. J. Neurophysiol. *70*, 387–396.

Koch, C., Poggio, T., and Torre, V. (1982). Retinal ganglion cells: a functional interpretation of dendritic morphology. Philos. Trans. R. Soc. Lond. (B) *298*, 227–263.

Koch, C., Poggio, T., and Torre, V. (1983). Nonlinear interactions in a dendritic tree: localization, timing, and role in information processing. Proc. Natl. Acad. Sci. USA *80*, 2799–2802.

Lambert, N. A., and Wilson, W. A. (1993). Heterogeneity in presynaptic regulation of GABA release from hippocampal inhibitory neurons. Neuron *11*, 1057–1067.

Llano, I., and Gerschenfeld, H. M. (1993). Inhibitory synaptic currents in stellate cells of rat cerebellar slices. J. Physiol. *468*, 177–200.

Major, G., Larkman, A. U., Jonas, P., Sakmann, B., and Jack, J. J. B. (1994). Detailed passive cable models of whole-cell recorded CA3 pyramidal neurons in rat hippocampal slices. J. Neurosci. *14*, 4613–4638.

McBain, C. J., and Dingledine, R. (1992). Dual-component miniature excitatory synaptic currents in rat hippocampal CA3 pyramidal neurons. J. Neurophysiol. *68*, 16–27.

McBain, C. J., and Dingledine, R. (1993). Heterogeneity of synaptic glutamate receptors on CA3 stratum radiatum interneurones of rat hippocampus. J. Physiol. *462*, 373–392.

Miles, R., Tóth, K., Gulyás, A. I., Hajós, N., and Freund, T. F. (1995). Different functions for dendritic and somatic inhibitory cells of the hippocampus. J. Physiol. *480*, 32.

Mody, I., De Koninck, Y., Otis, T. S., and Soltesz, I. (1994). Bridging the cleft at GABA synapses in the brain. Trends Neurosci. *17*, 517–525.

Nicoll, R. A. (1994). Neuroscience: Cajal's rational psychology. Nature *368*, 808–809.

Nusser, Z., Roberts, J. D. B., Baude, A., Richards, J. G., Sieghart, W., and Somogyi, P. (1995). Immunocytochemical localisation of the α1 and β2/3 subunits of the $GABA_A$ receptor in relation to specific GABAergic synapses in the dentate gyrus. Eur. J. Neurosci., in press.

Otis, T. S., and Mody, I. (1992). Modulation of decay kinetics and frequency of $GABA_A$ receptor-mediated spontaneous inhibitory postsynaptic currents in hippocampal neurons. Neuroscience *49*, 13–32.

Otis, T. S., Staley, K. J., and Mody, I. (1991). Perpetual inhibitory activity in mammalian brain slices generated by spontaneous GABA release. Brain Res. *545*, 142–150.

Pearce, R. A. (1993). Physiological evidence for two distinct $GABA_A$ responses in rat hippocampus. Neuron *10*, 189–200.

Rall, W. (1977). Core conductor theory and cable properties of neurons. In *Handbook of Physiology, Section I: The Nervous System*. E. R. Kandel, ed. (Bethesda, Maryland: American Physiological Society), pp. 39–97.

Richards, J. G., Schoch, P., Haring, P., Takacs, B., and Möhler, H. (1987). Resolving $GABA_A$/benzodiazepine receptors: cellular and subcellular localization in the CNS with monoclonal antibodies. J. Neurosci. *7*, 1866–1886.

Scanziani, M., Capogna, M., Gähwiler, B. H., and Thompson, S. M. (1992). Presynaptic inhibition of miniature excitatory synaptic currents by baclofen and adenosine in the hippocampus. Neuron *9*, 919–927.

Schoch, P., Richards, J. G., Haring, P., Takacs, B., Stahli, C., Staehelin, T., Haefely, W., and Mohler, H. (1985). Co-localization of GABA receptors and benzodiazepine receptors in the brain shown by monoclonal antibodies. Nature *314*, 168–171.

Smetters, D. K., and Nelson, S. B. (1995). Electrotonic structure and synaptic variability in cortical neurons. In Computation and Neural Systems, J. Bower, ed. (Norwell, Massachusetts: Kluwer Academic Publishing).

Soltesz, I., and Deschênes, M. (1993). Low- and high-frequency membrane potential oscillations during theta activity in CA1 and CA3 pyramidal neurons of the rat hippocampus under ketamine-xylazine anesthesia. J. Neurophysiol. *70*, 97–116.

Soltesz, I., and Mody, I. (1994). Patch-clamp recordings reveal powerful GABAergic inhibition in dentate hilar neurons. J. Neurosci. *14*, 2365–2376.

Soltesz, I., and Mody, I. (1995). Ca^{2+}-dependent plasticity of miniature inhibitory postsynaptic currents following amputation of dendrites in central neurons. J. Neurophysiol., in press.

Spruston, N., Jaffe, D. B., Williams, S. H., and Johnston, D. (1993). Voltage- and space-clamp errors associated with the measurement of electrotonically remote synaptic events. J. Neurophysiol. *70*, 781–802.

Spruston, N., and Johnston, D. (1992). Perforated patch-clamp analysis of the passive membrane properties of three classes of hippocampal neurons. J. Neurophysiol. *67*, 508–529.

Staley, K. J., and Mody, I. (1991). Integrity of perforant path fibers and the frequency of action potential independent excitatory and inhibitory synaptic events in dentate gyrus granule cells. Synapse *9*, 219–224.

Staley, K. J., and Mody, I. (1992). Shunting of excitatory input to dentate gyrus granule cells by a depolarizing $GABA_A$ receptor-mediated postsynaptic conductance. J. Neurophysiol. *68*, 197–212.

Staley, K. J., Otis, T. S., and Mody, I. (1992). Membrane properties of dentate gyrus granule cells: comparison of sharp microelectrode and whole-cell recordings. J. Neurophysiol. *67*, 1346–1358.

Stern, P., Edwards, F. A., and Sakmann, B. (1992). Fast and slow components of unitary EPSCs on stellate cells elicited by focal stimula-

tion in slices of rat visual cortex. J. Physiol. *449*, 247–278.

Stuart, G. J., and Sakmann, B. (1994). Active propagation of somatic action potentials into neocortical pyramidal cell dendrites. Nature *367*, 69–72.

Turner, J. D., Bodewitz, G., Thompson, C. L., and Stephenson, F. A. (1993). Immunohistochemical mapping of gamma-aminobutyric acid type-A receptor alpha subunits in rat central nervous system. Psychopharmacol. Ser. *11*, 29–49.

Ulrich, D., and Lüscher, H.-R. (1993). Miniature excitatory synaptic currents corrected for dendritic cable properties reveal quantal size and variance. J. Neurophysiol. *69*, 1769–1773.

Vu, E. T., and Krasne, F. B. (1992). Evidence for a computational distinction between proximal and distal neuronal inhibition. Science *255*, 1710–1712.

Williams, S. H., and Johnston, D. (1991). Kinetic properties of two anatomically distinct excitatory synapses in hippocampal CA3 pyramidal neurons. J. Neurophysiol. *66*, 1010–1020.

Wisden, W., Laurie, D. J., Monyer, H., and Seeburg, P. H. (1992). The distribution of 13 $GABA_A$ receptor subunit messenger RNAs in the rat brain. I. Telencephalon, diencephalon, mesencephalon. J. Neurosci. *12*, 1040–1062.

Zimprich, F., Zezula, J., Sieghart, W., and Lassmann, H. (1991). Immunohistochemical localization of the alpha 1, alpha 2 and alpha 3 subunit of the $GABA_A$ receptor in the rat brain. Neurosci. Lett. *127*, 125–128.